Retinal pigment epithelium imaging with a graded-index fiber

Burnand Alexandre

UNIL | Université de Lausanne
Faculté de biologie
et de médecine

UNIVERSITE DE LAUSANNE - FACULTE DE BIOLOGIE ET DE MEDECINE

Hôpital ophtalmique Jules-Gonin
Service Universitaire d'Ophtalmologie

Retinal pigment epithelium imaging with a graded-index fiber

THESE

préparée sous la direction du Professeur Thomas Wolfensberger
avec la co-direction du Professeur Demetri Psaltis

et présentée à la Faculté de biologie et de médecine de
l'Université de Lausanne pour l'obtention du grade de

DOCTEUR EN MEDECINE

par

Alexandre Burnand

Médecin diplômé de la Confédération Suisse
Originaire de Bioley-Magnoux (Vaud)

Lausanne

2022

UNIL | Université de Lausanne

Faculté de biologie et de médecine

Ecole Doctorale
Doctorat en médecine

Imprimatur

Vu le rapport présenté par le jury d'examen, composé de

Directeur.trice de thèse	Prof. **Thomas Wolfensberger**
Co-Directeur.trice de thèse	Prof. **Demetri Psaltis**
Expert.e	Prof. **Chiara Eandi**
Vice-Directeur de l'Ecole doctorale	Prof. **John Prior**

la Commission MD de l'Ecole doctorale autorise l'impression de la thèse de

Monsieur Alexandre Burnand

intitulée

Retinal pigment epithelium imaging with a graded-index fiber

Lausanne, le 29 septembre 2022

pour Le Doyen
de la Faculté de Biologie et de Médecine

Monsieur le Professeur John Prior
Vice-Directeur de l'Ecole doctorale

Résumé :

La rétine est structure complexe constituée de différentes couches de cellules, elle se compose en premier lieu de la neurorétine et de l'épithélium pigmentaire. La neurorétine est constituée principalement des photorécepteurs, des cellules bipolaires et des cellules ganglionnaires. Les photorécepteurs transforment l'information lumineuse en information électrique qui sera transmise via les cellules ganglionnaire dans le nerf optique. L'épithélium pigmentaire est une couche monostratifiée en contacte de la neurorétine, sa fonction principale est l'absorption de la lumière, le transport épithélial, la phagocytose des segments externe des photorécepteurs et l'isomérisation du 11-cis retinol pour le cycle visuel.

Avec le vieillissement, les produit de dégradation de la phagocytose des photorécepteurs vont produire de la lipofuscine qui va s'accumuler dans les cellules de l'épithélium pigmentaire. Une anomalie de l'épithélium pigmentaire ou une accumulation pathologique de lipofuscine peut être lié dans l'étiologie de rétinopathie. La lipofuscine est notamment un grand facteur de risque pour la dégénérescence maculaire atrophique ou dans la maladie de Stargardt.

L'observation de l'épithélium pigmentaire ainsi que la distribution de lipofuscine intracellulaire présente donc un intérêt pour la détection des premiers signes de maladies rétinienne et pour la compréhension de mécanisme cellulaire non accessible avec les méthodes d'observation usuelles. En ophtalmologie clinique, l'épithélium pigmentaire s'observe grâce à l'autofluorescence de la lipofuscine. Cette technique non invasive donne une image globale du fond d'œil mais ne permet malheureusement pas d'obtenir une résolution cellulaire.

Dans ce travail de thèse, nous vous présentons une nouvelle modalité d'imagerie permettant d'imager l'épithélium pigmentaire avec une résolution cellulaire, nous avons créé un endoscope composé d'une fibre optique GRIN permettant d'imager ex-vivo l'épithélium pigmentaire. Les fibres optiques à gradient d'indice (GRIN) habituellement utilisée pour les communication longue distance, peuvent également servir d'outils pour l'observation de tissus biologique.

Le système crée et composé d'une source laser, d'un miroir dichroïque, d'un capteur et d'un ordinateur pour l'analyse des données. Le système optique permet d'obtenir une résolution latérale de 0.37 µm, une résolution axiale de 3 µm et un champ de vision de 100 x 100 µm.
La résolution obtenue est suffisante pour visualiser ex-vivo les cellules de l'épithélium pigmentaire ainsi que la distribution de lipofuscine. La principale limitation de notre endoscope est une profondeur de champs limitée à env. 80 µm rendant l'excès à l'épithélium pigmentaire possible in-vivo uniquement avec un amincissement de la neurorétine ou à travers une déchirure rétinienne. Cette limitation est due au faible diamètre de la sonde utilisée (1.4 mm). La fabrication par les industries de sonde avec un diamètre plus important permettrait de contrecarrer cette limitation en dépit d'une procédure plus invasive.

Introduction:

Retinal imaging is important for diagnosis, understanding and follow-up for numerous ocular diseases like glaucoma, age-related macular degeneration (AMD) and diabetic retinopathy (LaRocca F, 2016). Different devices have been developed to observed the retina in clinic, like conventional color fundus imaging, optical coherence tomography (OCT), autofluorescence and confocal scanning laser ophthalmoscopy (SLO). These techniques image specific retinal structures (blood vessel, retinal layer, optic nerve) with specific lateral (i.e., in the x and y directions) and axial resolution (z direction). The light recorded for imaging emerging from the pupil is back-scattered or back-reflected by the different retina layers.

Imaging the interior of the eye (the Fundus) is a technical challenge first because the illumination light, as well as the light reflected by the retina must cross the pupil, which limits the numerical aperture (NA). Secondly it is challenging since the retina layers are mostly transparent tissue. This transparency property is important because light need to cross its full thickness before being absorbed by the photoreceptor (fig. 1) but this transparency also imposes difficulty to observe the retina. Without fluorescent antibody markers or staining it is very difficult to make accurate measurements of retina cells. (Ethan A. Rossi, 2017).

Recently some new imaging modalities have been developed to visualize the retinal pigment epithelium (RPE) cells, like adaptive optics optical coherence tomography (AO-OCT) or transscleral optical phase imaging (TOPI) (Laforest, 2020). Theses new modalites are only available in some research center and their resolution didn't permet to visualize the intracellular lipofucine distribution or nucleus. Having a cellular resolution with intacellular lipofuscin distibution present a great interest for detection and monitoring some RPE-retinal disease because early manifestation of RPE disease occurs at the cellular level.

RPE autofluorescence imaging and lipofuscin function

The retina is a complex structure, composed of eleven distinct layers (Jonnal RS, 2016) and has a total thickness in humans between 200 to 300 µm (fig. 1). The blood supply of the retina comes 2/3 from the choroid and 1/3 from the central retina artery. The retina is found above the RPE (Olaf, 2005). RPE is a single layer of polygonal cells with different functions (Simó R, 2010): (1) absorption of light and light scattering reduction within the eye, (2) phagocytosis outer segment of photoreceptor and breakdown in the lysosome, (3) isomerization of all-trans-retinaldehyde essential for the visual cycle, (4) transepithelial ions, water and nutriments transport to the retina.

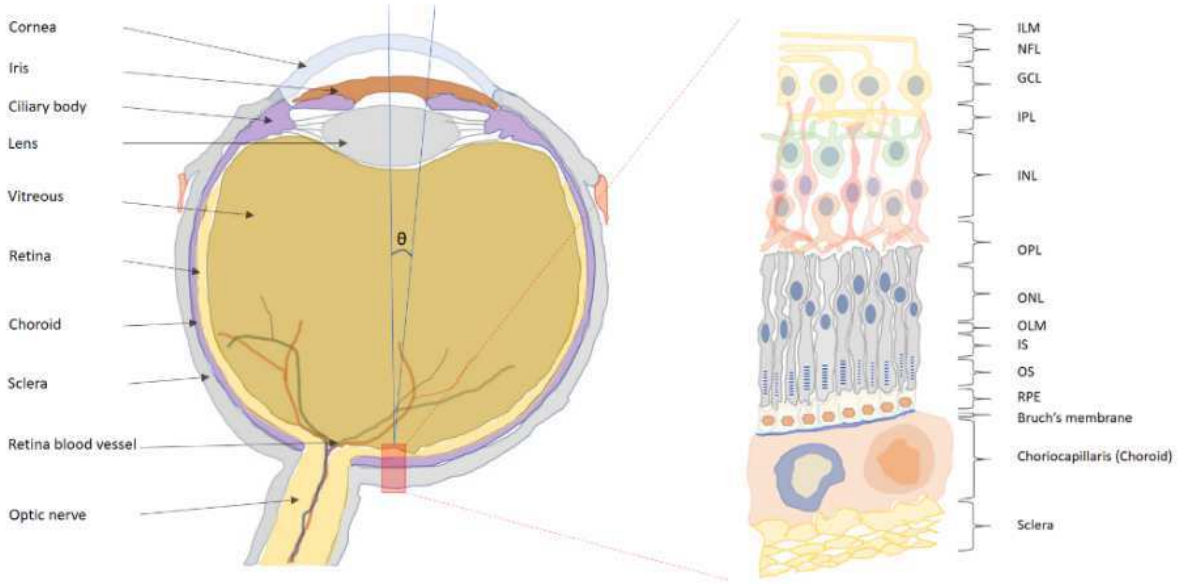

Figure 1: Eye and retina anatomy. Pupil's diameter limited the numerical aperture of the eye. ILM, inner limiting membrane; NFL, nerve fiber layer; GCL, ganglion cell layer; IPL, inner plexiform layer; INL, inner nuclear layer; OPL, outer plexiform layer; ONL, outer nuclear layer; OLM, outer limiting membrane; IS, inner segment; OS, outer segment; RPE, retinal pigment epithelium

RPE can be visualize with a technique called fundus autofluorescence (FAF or FA). This is an imaging modality that uses natural fluorescence in the RPE to generate an image. Fluorescence in the retina comes mainly from lipofuscin that is stored inside the lysosomes of RPE cells (Staudt S, 2000). Lipofuscin fluorescence are invisible to ophthalmoscopy and standard color fundus photography because FAF need dichroic filter.

The normal RPE fluorescence yields a slightly granular grey AF glow in contrast to the optic disc and retinal blood vessels which appear black (fig. 2A). Lipofuscin accumulation result of the incomplete phagocytosis or recycling of the retinal in the RPE (Davies S, 2001) and suggests RPE dysfunction or stress, this result in areas of bright white signal. Decreased FAF suggest loss of RPE cells and correlates to reduced levels of lipofuscin (fig. 2B). This result in areas of dark grey or black signal. Lipofuscin can inhibit normal RPE function due to their toxicity. This toxicity will cause RPE cell death and geographic atrophy. They also reduce retinal barrier function because the tight junction cannot close and separated from the choroid.

With aging there is free radical injuries and there is lipofuscin accumulation in the RPE cell (Sepah YJ, 2014) due to incomplete metabolism breakdown. Lipofuscin accumulation may also reflect pathological processes like in Stargardt's disease or in dry AMD (Kennedy CJ, 1995). Fundus autofluorescence gives information to the clinician and is an essential tool for evaluating some retinal diseases.

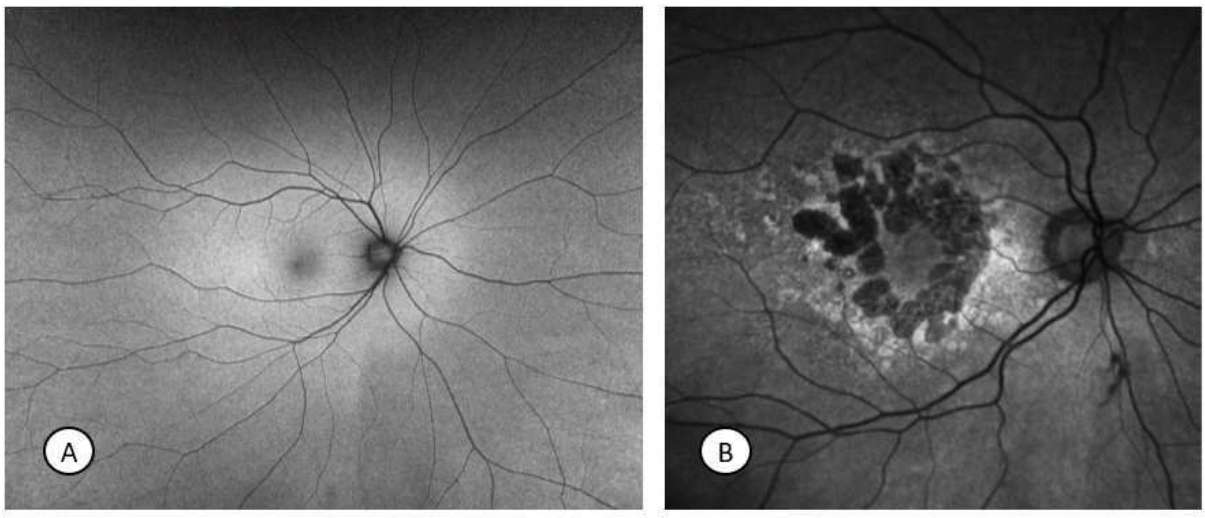

Figure 2: A) normal autofluorescence image of a right eye obtained with an Optos (Nikon). The optic disc appears black due to absence of lipofuscin. The fovea appears hypo-autofluorescent due to xanthophyll pigment that absorb light. Blood vessel appear dark since blood absorb excitation light. B) FAF in patient with geographic atrophy in advanced dry AMD showing hypo-AF area representing RPE atrophy surrounded by hyper-AF area representing RPE stress. (Courtesy of Brad Bowling, from Kanski's Clinical Ophthalmology, a systematic approach, eight edition)

Optical limitation in retina imaging:

All images obtained in clinic like fundus photography, OCT or FAF are limited by the optical property of the eye because the detector is outside the eyeball (Lakshminarayanan, 2015).
Transverse resolution is limited as in every optical system like microscopes by the finite aperture of the pupil which imposes a fundamental diffraction limited resolution (fig. 1). The light passing through the pupil interferes with itself creating an Airy pattern (Sanderson, 1999). The diffraction limited resolution is defined by Rayleigh criterion, that can be link with the NA of the eye.

$$d_{min} = \frac{1{,}22 \cdot \lambda \cdot f}{n \cdot D} = \frac{0.61 \cdot \lambda}{NA}$$

$d_{min} = minimal\ distance\ to\ distinguish\ two\ close\ objects\ [m]$
$\lambda = wavelength\ [m]$
$f = focal\ of\ the\ lens\ [m]$
$D = diameter\ of\ the\ pupil\ [m]$
$n = refractive\ index\ of\ the\ medium$ (1.33 for the vitreous body)
$NA = n \cdot sin(\theta)$
$\theta = half\ angle$

We can increase the resolution, if we increase the NA by using a mydriatic drop. The NA of the human eye ranges from 0.06 to 0.2 (2 to 7 mm pupil diameter, with f = 22.6 mm and λ = 550 nm). Theses NA are small compared to some microscopes immersion objective that can have NA bigger than 1.
However, although with a large pupil diameter, spatial resolution become limited by aberration, introduced by the lens, the cornea and the vitreous body (Larichev AV, 2002). To achieve optimum resolution across dilated pupil, adaptive optics (AO) has been used successfully. AO reduces the effects of optical aberrations and can provide transverse resolution close to the diffraction limited resolution

(table 1). This is enough to observe photoreceptor cells in the human retina (Lombardo M, 2012). Table 1: Resume resolution obtained with different device in ophthalmology:

	Transverse resolution	Axial resolution	FOV
Ophthalmoscopy direct	70 µm		~ 3 mm
Ophthalmoscopy indirect	200 µm (Onofrey, 1998)		~ 20 mm
FAF	10-20 µm		~ 30 mm
OCT	10-15 µm	1-15 µm (Fujimoto JG, 2000)	~ 9 mm
OCT + AO	2-3 µm	4.5 µm (Pircher M, 2017)	~ 1 mm

Table 1: Ophthalmoscopy, OCT and autofluorescence resolution. Transverse resolution determines with which size features can be identified.

Graded-index fiber endoscope:

The devices commonly used in eye examinations are non-invasive and record information from the outside of the eye through the pupil. To increase the resolution, we explore the possibility to record information from the inside of the eye with an endoscope that bypasses the pupil diameter limitation. Thin optical fiber probes can be used to imaged tissue in-vivo with minimum organ damage.

During vitrectomy surgery some openings are made in the pars plana area. We propose to use these openings to introduce a fiber endoscope and image cells close to the retina. A GRIN fiber or lens is the best candidate. Contrary to a step-index multimode fiber, a GRIN lens can produce images directly and does not need complex processing to compensate modal dispersion.

The endoscope combines a GRIN objective lens and a GRIN relay enveloped through a stainless-steel holder (Peter H. Tran, 2004). The objective lens with a diameter of 1.4 mm and a NA of 0.8 created image at the exit surface of the objective lens, which will be transferred by the relay lens and finally recorded by a camera system (fig. 3).

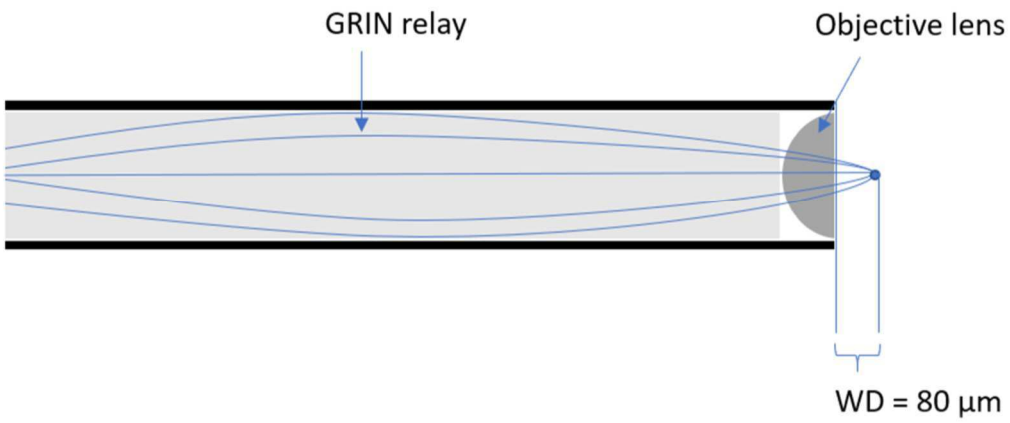

Figure 3: Endoscopic imaging objective: GRINTECH fiber, object NA = 0.8, object working distance 80 µm (water), Diameter=1.4 mm

The GRIN fiber has a refractive index profile that varies smoothly in the radial direction (fig. 4). The refractive index profile has nearly a parabolic shape, decreasing with radial distance from the center of the core. The light rays periodically and follow a sinusoidal path down the fiber (see appendix). The variation of the refractive index induces focusing light in a way similar to a conventional lens.

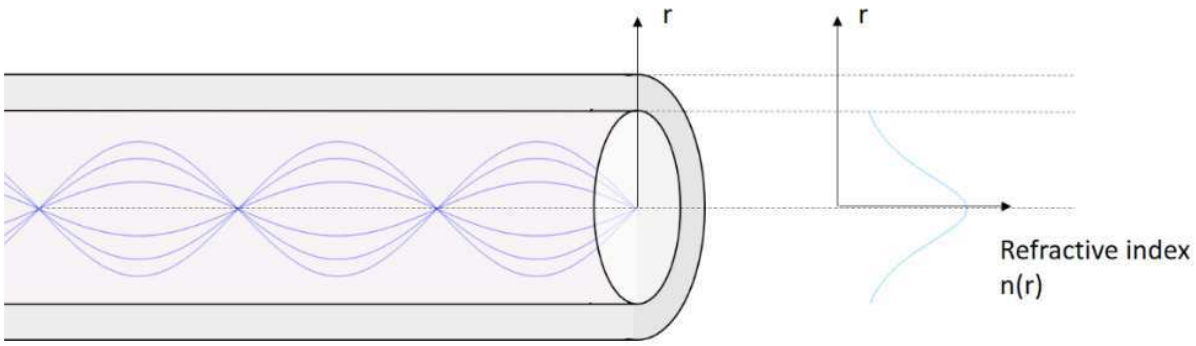

Figure 4: GRIN fiber, refractive index is maximal at the center and decrease as radius increase.

$$n(r) = n_0 \cdot sech(g \cdot r) = \frac{n_0}{cosh(g \cdot r)}$$

n_0: refractive index at the center of the fiber

g: geometrical gradient constant (steepness of the GRIN lens)

r: radius of the fiber

Material and methods:

Experimental setup:

The experimental setup we use for retina imaging is shown in figure 5. We used collimated light from an argon ion laser emitting continuous-wave output at λ=488nm. The excitatory light is injected in a long pass dichroic mirror (DMLP505T, reflection band 380-490 nm, transmission band 520-800 nm). Excitation light is then reflected into the galvo-mirror that can precisely position the laser beam and are used for scanning the sample. After galvo-mirror, the beam reaches the objective (20x, NA = 0.35) which focus the light in the GRIN fiber to reach the sample. The excitatory light excited the fluorophore in the sample, and emitted fluorescence transmitted back through the objective that magnified and through the dichroic mirror into the photon counting detector (MPD with high photon detection efficiency). All experiments and methods used on rat was performed in accordance with guidelines of the EPFL. Labview (National Instruments) is used for galvo-mirror control and data acquisition.

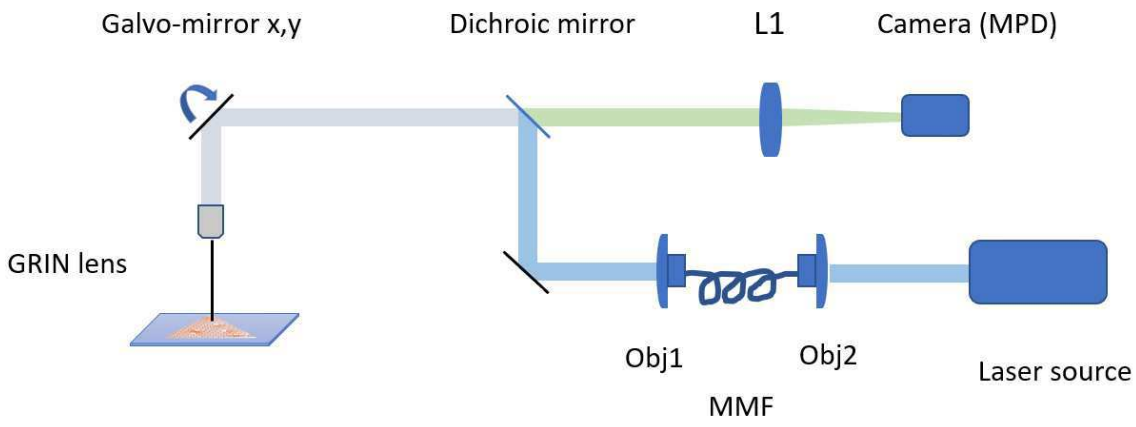

Figure 5: Experimental setup for retina imaging. The laser beam is injected into the multimode fiber to reach the dichroic mirror. Obj, microscope objective lens; MMF, multimode fiber; L, lens

Sample preparation protocol:

An albino rat under general anesthesia was sacrificed with injection of potassium chloride directly in the heart. After cessation of heart activity, the eyes were enucleated and placed into a holder with a buffer solution of phosphate-buffered saline (PBS). After making a hole in the limbus, the tissue was fixed with paraformaldehyde (PAF) 4% for 30 minutes at room temperature and washed with PBS (PAF can have a little auto-fluorescence). The sample was then submerged in PBS to maintain its spherical shape.

We remove the cornea, the lens and the extraneous tissue from the outside of the eye. The eyeball was cut with a scissor perpendicular to the limbus toward the optic nerve head. The eye was open like a flower structure with forceps and small scissors. We grasped a petal of the neuroretina and pulled the neuroretina away from the RPE with forceps and paintbrush.

The sample was fixed again with PAF4% during 10 minutes and washed with PBS to remove the debris. We made staining for 5 minutes with DAPI (1:5000) followed by washing for 3 x 10 minutes in PBS. The RPE sample was finally transferred onto a glass slide.

Results:

The quality of the rat RPE samples was checked with a conventional confocal microscope (Zeiss 710 confocal microscope) with excitation wavelength similar than in our experimental setup (i.e., 488nm) (fig. 6). In fluorescence mode, the signal comes from lipofuscin that accumulates in the RPE cytoplasm. RPE consists of monolayer of cuboid cells. The nucleus appeared black due to lack of lipofuscin in the nucleus. We observed a majority multinucleate RPE cell, a phenomenon that occur with aging. We did not observe any cell with more than 2 nuclei. Cells with two nuclei are generally larger than cells with a single nucleus.

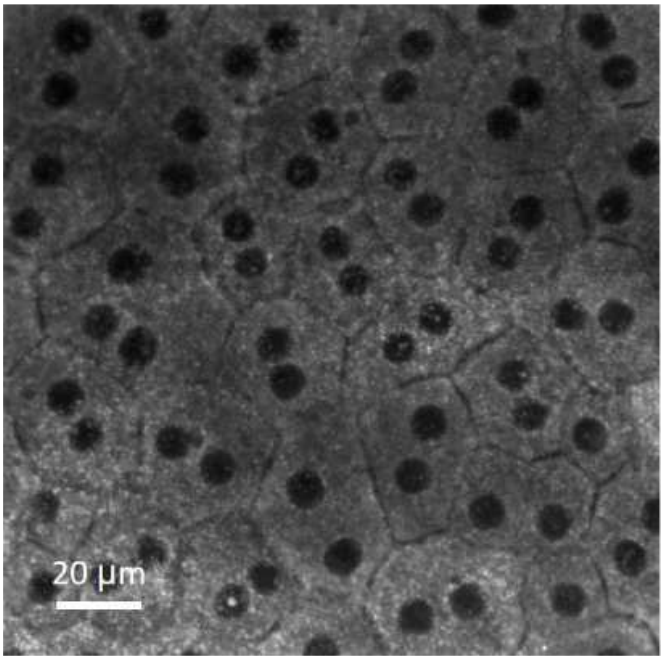

Figure 6: Rat RPE imaged with confocal LSM710 microscopy, excitation of 488nm, detection range: 497-735nm, oil immersion objective 40x, NA=1.3, field of view= 155µm x 155µm

Autofluorescence spectra of RPE cells associated with lipofuscin are measured with the Zeiss confocal LSM710 microscopy equipped with a spectrophotometer at 5 nm wavelength intervals between 494 and 689 nm. The tissue samples were excited at 488nm, emission spectra were measured and presented in fig. 7. We notice that lipofuscin emission spectra are broad and had a maximal intensity between 560 to 610nm (in the yellow range).

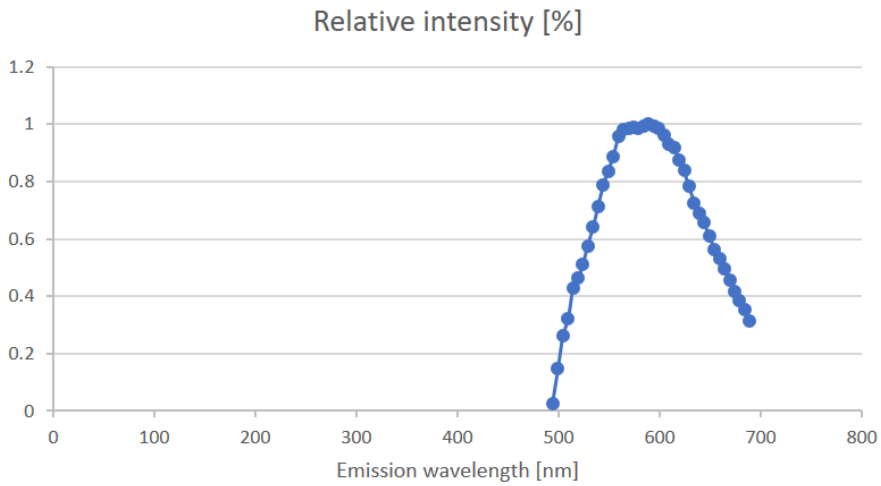

Figure 7 : Lipofuscin fluorescent emission spectra. We observed a pic emission in the yellow range.

Figure 8 present the rat RPE imaged with an oil immersion objective (NA = 1.4). We have made this image to test the correct alignment and functionality of the experimental setup presented in fig. 5. Figure 9 shows the image obtained with the GRIN probe. Figure 10 shows the sample in reflectance mode. The contrast in the reflectance confocal microscopy images is due to the difference in the light reflected from different parts of the sample. Strongly reflecting structures appear bright and non-reflecting structure appear dark. The cell's membrane is clearly visible; however, a weak signal also comes from the cytosol.

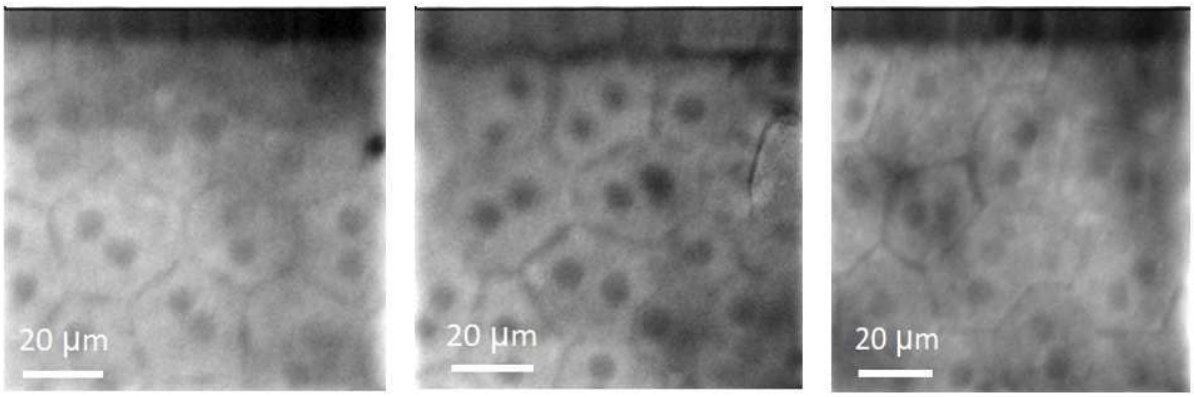

Figure 8: Rat RPE imaged with our experimental setup with an immersion objective NA= 1.4, excitation wavelength = 488nm, field of view = 100 µm x 100 µm.

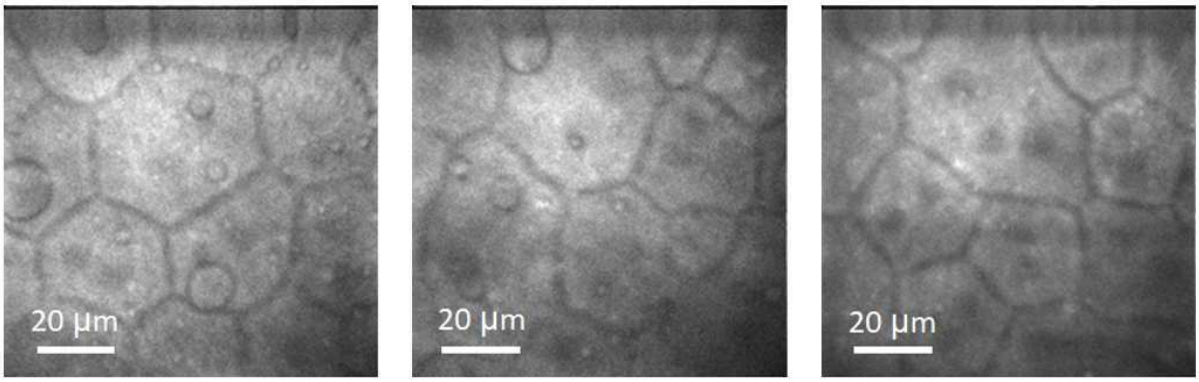

Figure 9: Rat RPE imaged with our experimental setup with GRIN probe NA=0.8, excitation wavelength = 488nm, field of view = 100 µm x 100 µm.

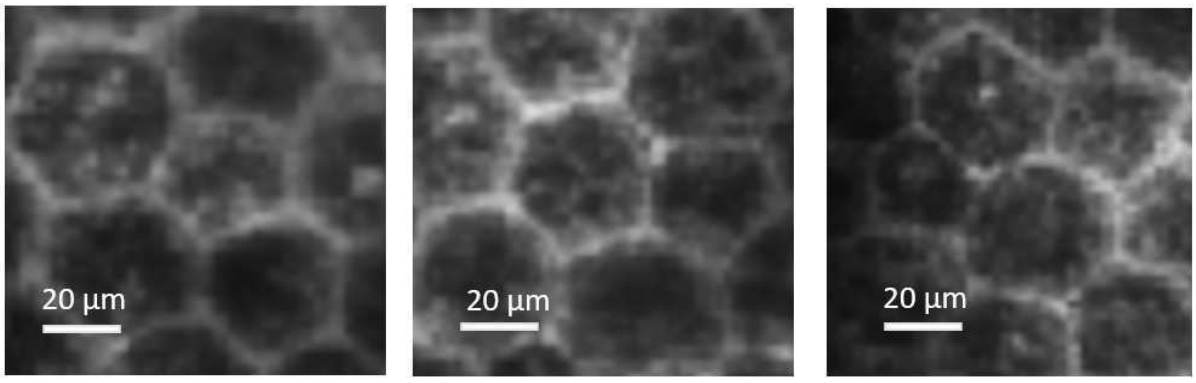

Figure 10: Rat RPE imaged on reflectance confocal mode, with GRIN probe NA = 0.8. Cell membrane are hyperreflective and appears white, cytosol is hypo-reflective and appears black, field of view = 100 µm x 100 µm.

Discussion:

This study shows that a 3 cm GRIN fiber permits fluorescent ex-vivo RPE cells imaging with a cellular resolution. This imaging new modality give a better resolution compared to other RPE imaging like AO-OCT or TOPI. All imaging modalities have their advantages and disadvantage AO-OCT and TOPI are non-invasive methods, but they didn't allow to observed the RPE nucleus. A GRIN fiber based on fluorescence mode allow visualization of the nucleus whereas AO-OCT or TOPI only give information about the cell boundaries. Figure 11 shows human RPE imaged with TOPI (fig. 11A) and with AO-OCT (fig. 11B).

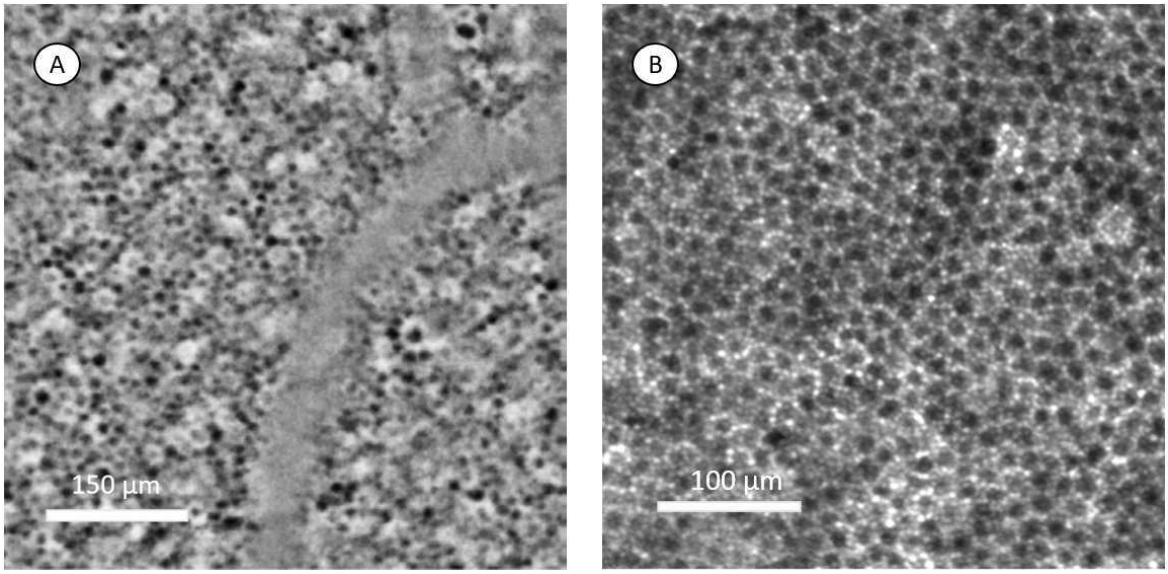

Figure 11: A) Human RPE mosaic imaged with transscleral optical phase (TOPI) (Laforest T. 2020); B) Human RPE mosaic imaged with AO-OCT (Kurokawa K, 2021)

The NA determines the ability to resolve small detail, image quality is directed link to the NA. We can observe more detail with a NA of 1.4 corresponding to an immersion lens instead a NA of 0.8 corresponding to our GRIN lens. The performance of our GRIN probe with a NA of 0.8 is good enough to observed clearly cytoplasm in fluorescence mode and the cell membrane in reflectance mode. In practice, the WD is an important parameter when the object of interest is located below structure like different retinal layer.

We try to make imaging with fiber on a whole pig eye, with an opening in the same way as during vitreo-retina surgery, where the instruments are introduced into the eye through the pars plana. We noticed that our probe doesn't allow to image RPE cell in vivo, due to different restriction: the main limitation is the working distance (WD), our probe have a WD limited of 80 µm in water and the retina thickness is between 200 and 300 µm depending on the area of the retina. There exists some probe with higher WD up to 5mm, but NA is too low (0.15) not enough for cellular resolution.
Fiber design is a compromise exercise, a small diameter is less invasive, but have proportional smaller WD. We can also increase the WD by reducing the NA, but in this case we have also a reduction in

resolution (fig. 12). In order to have a WD of 300 µm and NA = 0.8 we need to have a fiber diameter of ≈ 5 mm, which is bigger than the classical opening surgery in the pars plana (27 gauge = 0.41 mm), this is invasive tools not adapted for modern surgery.

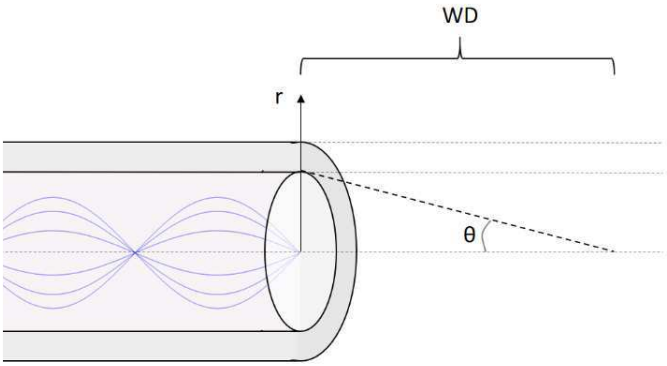

Figure 12: GRIN fiber: Working distance and numerical aperture. The WD is reduced when the NA increased.

Manufacturing a GRIN probe with a larger objective diameter that allowed a WD of 300 µm and a NA of 0.8 enable in theory to image in-vivo RPE under a retina. Having a cellular resolution level could be important for clinician in order to diagnose some retinal illness in early stage before macroscopic changed or visual function deterioration.

This device could also be used for gene transfer therapy for retinal dystrophy. It's become possible to observed and target the subretinal space for viral vector injection directly in the good space without damaging the neighbor area.

We try to make ex-vivo imaging in the whole eye without sample preparation mounted on glass to be close as possible as in the reality, but testing was also difficult, because retina without blood supply become rapidly opaque due to the death of the RPE cell, loss of vascularization compromises its transparency, this forms a strong scattering layer and avoid good signal from RPE.

However, our setup could be used in a specific patient with a pathologic eye disease called retina break in which there is a hole in the neuroretina and the RPE is directly accessible for imaging. If we pass off the sterility process and ethics commission, our endoscope can theoretically image human RPE in-vivo in these patients. We need to keep in mind, that the major limitation of this technique is that we need to go in the eye to image cell, this invasive and can have side effect like infection and the necessary of vitrectomy. That why this technique is limited for specific patient and can never be a large field diagnose tools.

Conclusion:

Retina imaging is a challenging because observation is limited by the eye NA, cornea and crystallin aberration and also because tissue is mostly transparent. To overtake these limitations, this study presented a GRIN fiber, that we used like an endoscope. This device providing a lateral resolution of 0.37 µm and permits RPE cellular resolution and lipofuscin distribution visualization. The major limitation of our device is the WD, actually the available probe has a WD of 80 µm this is not enough to reach the RPE in a healthy eye. Nevertheless, this new image modality could theoretically be used in specific patient with retina tears after a vitrectomy. This technique could be used in some specific situation. However, it's unfortunately not adapted for general follow-up.

Appendix:

We want to determine the ray trajectory in a GRIN fiber. In order to find the path, we need to use the concept of optical path length (OPL) and Fermat's principle.
Fermat's principle tells us that that the light rays travel along the path T_1 between the two points A and B, follow a path such that the time of travel between the two points is an extremum (smallest time) relative to all other possible neighboring paths: $T_2, T_3, ..$ (fig. 13).
In general, in an inhomogeneous medium the refractive index in a function of the position: $n(x, y, z)$

Therefore, the time taken by light to travel from the points A and B is given by:

$$OPL = \int_A^B n(x, y, z)dl \quad (1)$$

where dl is the differential element of length along a light path.

In a GRIN fiber the refractive index is hyperbolic, the refractive index profile can be expressed as

$$n(r) = n_0 \cdot \operatorname{sech}(g \cdot r) = \frac{n_0}{cosh(g \cdot r)} \quad (2)$$

where n_0 is the maximal refractive index in the center of the fiber, r is the radial distance from the center of the fiber and g is a gradient constant of the GRIN lens. Refractive index that decreases with increasing radial distance from the optical axis of the fiber (fig. 14).

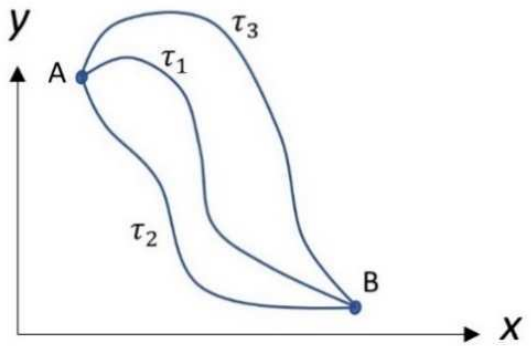

Figure 13: Different path ray possible between point A and point B

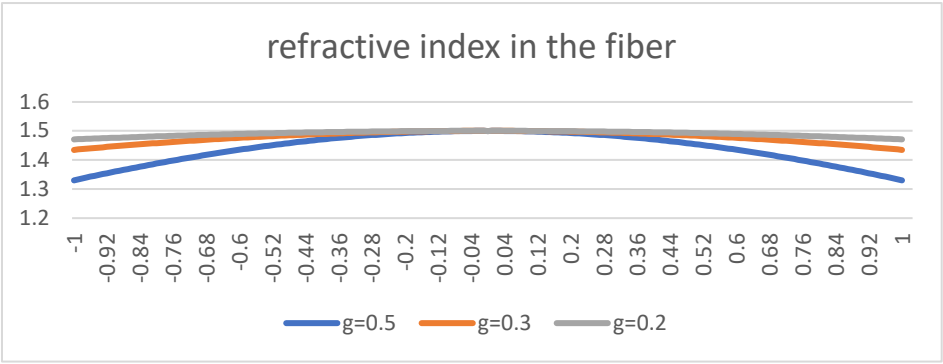

Figure 14: refractive index profile with respect to the radius with different gradient constant

Let defined a two-dimensional Euclidean coordinate system: $\mathbb{R}2$

To describe the ray trajectories. With two points $A(x;y)$ and $B(x;y)$. An extremum means that the rate of change is zero, i.e.:

$$\partial(OPL) = 0 <=> \partial \int_A^B n(x,y,z)dl = 0 \quad (3)$$

In a GRIN fiber refractive index varies only with respect to the radius. We took advantage of cylindrical symmetry to reduce the 3d to a 2d problem.

The optical path length OPL is proportional to the time required for the light to travel between two points and is simplified by:

$$OPL = \int_A^B n(y)dl = \int_A^B n(y)\sqrt{dx^2+dy^2} = \int_A^B n(y)\sqrt{dx^2\left(1+\frac{dy^2}{dx^2}\right)} = \int_A^B n(y)\sqrt{(1+y'^2)}dx = \int_A^B f(x,y,y')dx \quad (4)$$

with $dl = \sqrt{dx^2+dy^2} = \sqrt{dx^2\left(1+\frac{dy^2}{dx^2}\right)}$

Integral become: $OPL = \int_A^B f(x,y,y')dx$ solution of the integral is given by the Euler-Lagrange equation to attain an extreme value the extremizing function y(x) should satisfy (Amaranath, 2008):

$$\frac{\partial f}{\partial y} - \frac{d}{dx}\left(\frac{\partial f}{\partial y'}\right) = 0 \quad (5)$$

Here in GRIN fiber:

$$f(x,y,y') = \frac{n_0}{cosh(g\cdot y)}\sqrt{(1+y'^2)} \quad (6)$$

Differentiating (6) partially with respect to y and y', we get

$$\frac{\partial f}{\partial y} = \frac{-g\cdot n_0\cdot \sinh(g\cdot y)\sqrt{1+y'^2}}{\cosh^2(g\cdot y)} \quad (7)$$

$$\frac{\partial f}{\partial y'} = \frac{n_0\cdot y'}{cosh(g\cdot y)\cdot\sqrt{1+y'^2}} \quad (8)$$

$$\frac{\partial}{\partial x}\left(\frac{\partial f}{\partial y'}\right) = \frac{\partial}{\partial x}\left(\frac{n_0\cdot y'}{cosh(g\cdot y)\cdot\sqrt{1+y'^2}}\right) = \frac{n_0\left[\left(y''\cosh(g\cdot y)(1+y'^2) - y'\sinh(g\cdot y)gy'\left(1+y'^2\right) - \cosh(gy)y'^2y''\right]}{cosh^2(g\cdot y)\cdot(1+y'^2)^{3/2}} \quad (9)$$

Substituting (7) and (9) in (5), we have (10)

$$\frac{-g\cdot n_0\cdot \sinh(g\cdot y)\sqrt{1+y'^2}}{\cosh^2(g\cdot y)} - \frac{n_0\left[\left(y''\cosh(g\cdot y)(1+y'^2)\right) - y'\sinh(g\cdot y)gy'\left(1+y'^2\right) - \cosh(gy)y'^2y''\right]}{cosh^2(g\cdot y)\cdot\left(1+y'^2\right)^{\frac{3}{2}}} = 0 \quad (10)$$

The algebra is obtained is not trivial, but we can simplify considerably when the paraxial approximation is used (Bahaa E. A. Saleh, 2007).

In the paraxial approximation, the trajectory is almost parallel to the y axis, thus: $y' \cong 0$ (11)

And the equation become: $\frac{-g \cdot n_0 \cdot \sinh(g \cdot y)}{\cosh^2(g \cdot y)} - \frac{n_0[(y'' \cosh(g \cdot y)]}{cosh^2(g \cdot y)} = 0$ (12)

$$y'' + g \cdot \tanh(g \cdot y) = 0 \quad (13)$$

$\tanh(gy) \approx gy$ if $y \ll 1$

$$y'' + g^2 y = 0 \quad (14)$$

Assuming an initial position $y(0) = y_0$ and initial slope $\frac{dy}{dx} = \theta_0$ at x=0

$$y(x) = y_0 \cos(gx) + \frac{\theta_0}{g} \sin(gx) \quad (15)$$

The solution is harmonic function with a period of $\frac{2\pi}{g}$ known as the pitch

Acknowledgements:

I would like to acknowledge Prof. Demetri Psaltis (Optics Laboratory – EPFL) and her team that give me the opportunity to make this research in their laboratory in collaboration with the Jules-Gonin ophthalmic hospital. I would like also to acknowledge Prof. Behar-Cohen (Hotel-Dieu de Paris - Hôpital Cochin) and her team for her insights in the sample preparation.

Abbreviations:

AMD	age-related macular degeneration
AO	adaptive optics
DAPI	4',6-diamidino-2-phenylindole
DPC	digital face conjugaison
FAF	fundus autofluorescence
FOV	field of view
GRIN	Graded-index
NA	numerical aperture
OCT	optical coherent tomography
OPL	optical path length
PAF	paraformaldehyde
PBS	phosphate-buffered saline
RPE	Retinal pigment epithelial
SLO	confocal scanning laser ophthalmoscope
WD	working distance
TOPI	transscleral optical phase imaging

References:

Amaranath T. An Elementary Course in Partial Differential Equations. 2nd ed. Alpha Science International; 2003.

Bahaa E. A. Saleh, M. C. Fundamental of Photonics. 2nd ed. chap. 1. Wiley-Interscience; 2007.

Davies, S et al. Photocytotoxicity of lipofuscin in human retinal pigment epithelial cells. Free radical biology & medicine vol. 31,2 (2001)

Ethan A. Rossi, C. E. Imaging and Quantifying Ganglion Cells and Other Transparent Neurons in the Living Human Retina. Proceedings of the National Academy of Sciences of the United States of America; 2017.

Fujimoto JG, P. C. Optical coherence tomography: an emerging technology for biomedical imaging and optical biopsy. Neoplasia; 2000.

Jonnal RS, K. O. A Review of Adaptive Optics Optical Coherence Tomography: Technical Advances, Scientific Applications, and the Future. Technical Advances, Scientific Applications, and the Future. Invest Ophthalmol Vis Sci; 2016.

Kennedy CJ, R. P. Lipofuscin of the retinal pigment. Eye (Lond); 1995.

Kurokawa K. Multi-reference global registration of individual A-lines in adaptive optics optical coherence tomography retinal images. J Biomed Opt. 2021

Laforest, T. Transscleral Optical Phase Imaging of the Human Retina. Nature Photonics, 439–445; 2020.

Lakshminarayanan, M. R. Human Vision and Perception. Handbook of Advanced Lighting Technology; 2015.

Larichev AV, I. P. Adaptive System for Eye-Fundus Imaging. Quantum Electron; 2002.

LaRocca F, N. D. In vivo cellular-resolution retinal imaging in infants and children using an ultracompact handheld probe. Nat Photonics. 2016; 10:580-584. doi: 10.1038/nphoton.2016.141.

Lombardo M, S. S. Adaptive optics technology for high-resolution retinal imaging. Sensors (Basel); 2012.

Olaf, S. The Retinal Pigment Epithelium in Visual Function. Physiol Rev 85; 2005.

Onofrey, B. E. Ocular therapeutics handbook: A clinical manual. Philadelphia. Lippincott Williams & Wilkins; 1998. p. 52.

Peter H. Tran, D. S. In vivo endoscopic optical coherence tomography by use of a rotational microelectromechanical system probe. Opt. Lett. 29; 2004.

Pircher M, Z. R. Review of adaptive optics OCT (AO-OCT): principles and applications for retinal imaging. Biomed Opt Express; 2017.

Sanderson, J. Introduction to Light Microscopy. Journal of Microscopy, 193: 90-91; 1999.

Sepah YJ, A. A. Sepah YJ, Akhtar A, Sadiq MA, et al. Fundus autofluorescence imaging: Fundamentals and clinical relevance. Saudi J Ophthalmol; 2014.

Simó R, V. M.-R. The retinal pigment epithelium: something more than a constituent of the blood-retinal barrier--implications for the pathogenesis of diabetic retinopathy. J Biomed Biotechnol; 2010.

Staudt S, B. C. Various intra-and extracellular fluorophores other than RPE-lipofuscin contribute to variations in spatial distribution and intensity in topographic fundus autofluorescence images. Invest Ophthalmol Vis Sci; 2000.